Chemical Engineering Journal 169 (2011) 270–281

Contents lists available at ScienceDirect

Chemical Engineering Journal

journal homepage: www.elsevier.com/locate/cej

Optimized design of an electrochemical filter-press reactor using CFD methods

Ángel Frías-Ferrer[a], Ignacio Tudela[a], Olivier Louisnard[b], Verónica Sáez[a], María Deseada Esclapez[c], María Isabel Díez-García[a], Pedro Bonete[c], José González-García[a,*]

[a] Grupo de Nuevos Desarrollos Tecnológicos en Electroquímica: Sonoelectroquímica y Bioelectroquímica. Departamento de Química Física e Instituto Universitario de Electroquímica. Universidad de Alicante. Ap. Correos 99. 03080 Alicante, Spain
[b] Ecole des Mines Albi, Centre RAPSODEE, Université de Toulouse, FRE CNRS 3213, 81013 Albi, France
[c] Grupo de Fotoquímica y Electroquímica de Semiconductores. Departamento de Química Física e Instituto Universitario de Electroquímica. Universidad de Alicante. Ap. Correos 99. 03080 Alicante, Spain

ARTICLE INFO

Article history:
Received 12 December 2010
Received in revised form 15 February 2011
Accepted 17 February 2011

Keywords:
CFD
Electrochemistry
Filter-press reactor
Hydrodynamics
Laminar flow
Mass transfer
RTD

ABSTRACT

A former laboratory filter-press electrochemical reactor previously used in electrodialysis, electrosynthesis and wastewater treatment was studied from a hydrodynamic point of view using computational fluid dynamics (CFD). A finite elements method (FEM) software environment was used in order to simulate both fluid velocity field and tracer diffusion in the reactor for different low Reynolds numbers, enabling the estimation of active and stagnant areas inside the reactor. These results provided interesting information in order to design a new electrochemical compartment focusing on the entrance-exit manifolds to minimize the formation of stagnant areas within the reactor. CFD methods were again employed to study and optimize the new reactor in order to predict its performance. In both cases, CFD calculations were compared with residence time distribution (RTD) studies in order to validate the simulations.

1. Introduction

Filter-press configuration is one of the most commonly and extensively studied for electrochemical reactors [1–6]. These systems usually consist of: (i) electrodes fitted in a parallel plate assembly, (ii) frames to hold the electrodes, and (iii) membranes in case of a system working in divided configuration. The fluid flow pattern affects the reactor performance and this pattern is mainly fixed by the design of the entrance-exit manifolds [7] and also by secondary processes which could take place in the reaction compartment (i.e. gas-evolving reactions [8]). According to this, a detailed study of these systems from a hydrodynamic point of view should be done, in order to obtain the fluid velocity profile and detect the stagnant zones and backmixing effects in the latter. The existence of these zones can become a problem for different electrochemical processes such as (i) synthesis, as the electrolyte can be poorly stirred, with the electroactive species being depleted without proper regeneration by fresh streams; secondary or side reactions can take place, decreasing the current efficiency and the purity of the final product [9]; (ii) gas-evolving processes, where gas can block the active electrode surface, promoting their local heating and corrosion [10]; and (iii) polymerization of by-products which can deposit onto the electrode surface [11].

Several experimental works can be found in literature, related to the study of the hydrodynamic behaviour and mass transport inside of electrochemical filter-press reactors [12–20] such as limiting current measurements or RTD studies, among other experimental procedures. Unfortunately, the information provided by these techniques may not be sufficient to completely understand the hydrodynamic behaviour of electrochemical filter-press reactors equipped with complex manifolds or turbulence promoters. Therefore, other methods must be used.

In the last years, computational fluid dynamics (CFD) has proved to be a helpful tool, enabling to simulate the hydrodynamic behaviour of different electrochemical systems [21–23], including filter-press reactors. Jomard et al. [24] studied the influence of the gas-evolving process in a laboratory filer-press electrolyser employed in the massive production of hydrogen (two phase flow hydrodynamic system). They focused on the gas production because the evolution of very fine hydrogen bubbles modified the local electrical conductivity of the electrolyte, while other aspects such as the influence of the entrance-exit manifolds geometry or fluid flow rate were not analyzed. Also, no comparison with experimental results was proposed. Santos et al. [25] analyzed the fluid flow regime and mass transport in a commercial filter press reactor and the results were compared to experimental measurements of pressure drop, limiting current values and

* Corresponding author. Tel.: +34 965903855.
E-mail address: jose.gonzalez@ua.es (J. González-García).

1385-8947/$ – see front matter © 2011 Elsevier B.V. All rights reserved.
doi:10.1016/j.cej.2011.02.053

Table 1
Dimensions for the UA63.03 and the UA63.04 electrochemical filter-press reactors.

Reactor	B (m)	L (m)	s (m)	d_e (m)	Le	$\gamma = s/B$
UA63.03	7.0×10^{-2}	9.0×10^{-2}	3.0×10^{-3}	0.58×10^{-2}	6.44×10^{-2}	4.29×10^{-2}
UA63.04	7.0×10^{-2}	9.0×10^{-2}	4.0×10^{-3}	0.76×10^{-2}	8.44×10^{-2}	5.71×10^{-2}

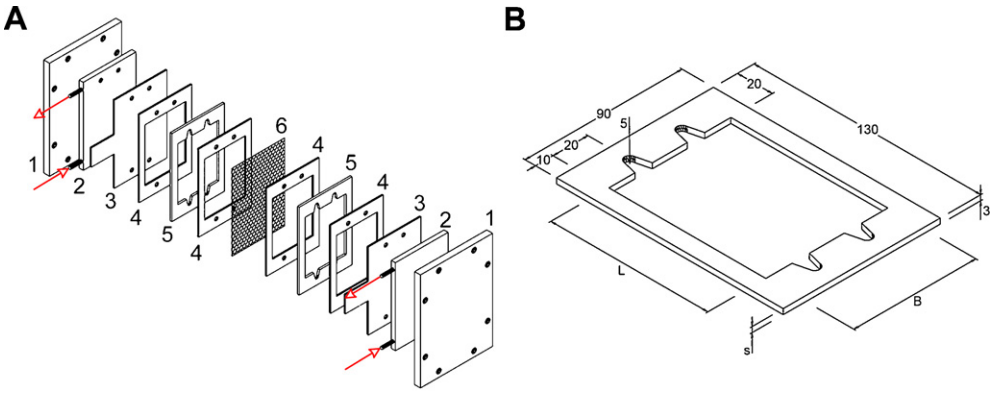

Fig. 1. (A) Exploded view of the UA63.03 electrochemical reactor in divided configuration: (1) holding plates, (2) polypropylene block with flow channels, (3) electrodes, (4) joints, (5) electrochemical compartments and (6) membrane. (B) View of the UA63.03 compartment showing the geometrical dimensions in mm, where B is the compartment width, L is the compartment length and s is the compartment thickness.

mass balance analyses. They followed a simpler approach of mono-phasic methodology despite the electrochemical reaction studied (electro-oxidation of pollutants) involved gas-evolving processes. This work also provided a more rigorous approach from a hydrodynamic point of view, as they took into account the inlet and outlet ports in the domain for the CFD studies. As a conclusion, they suggested that turbulent-developing flow in the studied electrochemical cell can be adequately described by mono-phasic CFD simulations, which significantly simplifies its mass-transport characterization and constitute a valuable tool for its optimization. Vázquez et al. [26,27] studied a different commercial filter-press reactor, obtaining information on the influence of the inlet and outlet manifolds, and the fluid developing zone. They also estimated mass transport coefficients from the CFD simulations, and compared them to experimental values through empirical correlations.

Former UA63.03 electrochemical reactor studied in this work was a laboratory filter-press reactor used for electrodialysis [28], wastewater treatments [11,29,30] and organic synthesis [31]. This electrochemical reactor was previously characterized by experimental RTD and mass transport studies, including limiting current techniques [7,32]. Preliminary CFD simulations of this reactor were already presented with promising results [33], where notorious stagnant areas were observed. Those basic results were confirmed in this work with further CFD studies, where the simulated fluid velocity field and tracer diffusion inside the non-optimized UA63.03 reactor were confronted to experimental RTD data from previous experimental work [32] in order to validate CFD simulations. From that point, our goal was to entirely develop a new electrochemical reactor employing CFD techniques step-by-step: from the first preliminary design to the last prototype actually built, each of the different modifications introduced in the geometry was

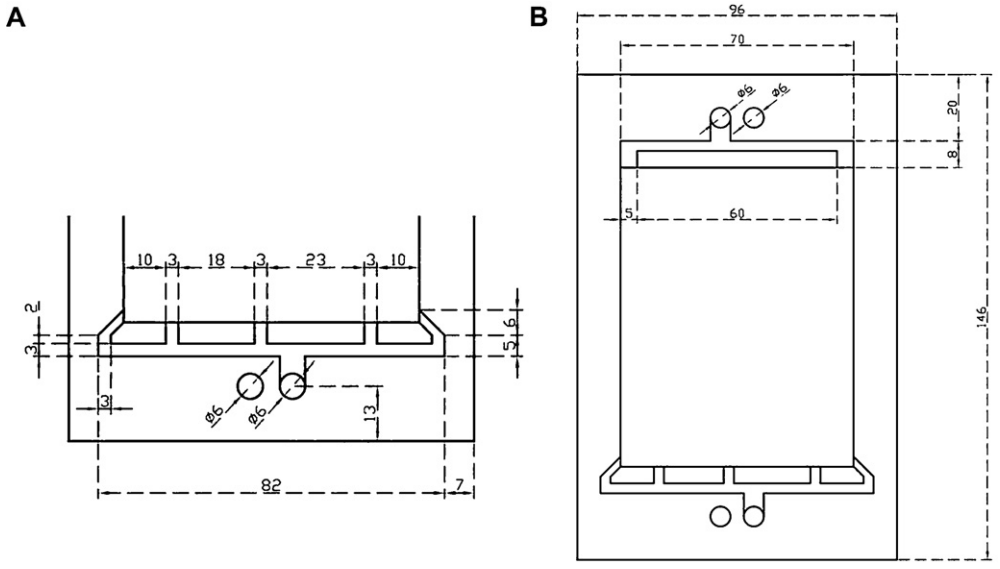

Fig. 2. (A) Detailed view of the entrance manifold in the newly designed UA63.04 electrochemical reactor. (B) General view of the UA63.04 compartment. All the geometrical dimensions are in mm.

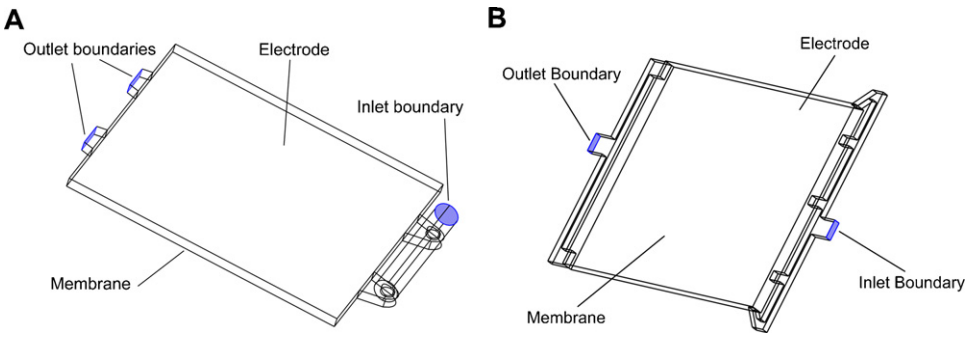

Fig. 3. Geometry for CFD simulations: (A) UA63.03 compartment, (B) UA63.04 compartment. Inlet and outlet boundaries are highlighted. The remaining boundaries are considered as non-slip walls.

tested with CFD methods from a hydrodynamic point of view in order to probe whether those modifications were optimizing the flow regime or not. This procedure led to the current design of the UA63.04 compartment, which was experimentally validated with RTD studies. For that purpose, no turbulent promoters were used, since the aim of this study was to make an initial approach to the design of a filter-press reactor by CFD methods. Turbulence promoter studies are generally focused on individual promoter cells [34], assuming a fully developed flow in order to analyze shear stress and enhanced mass transport rates near membranes or the electrodes, while the intention of this work is the study of the fluid dynamics inside the reactor at a larger scale.

2. Material and methods

2.1. The reactors

2.1.1. The UA63.03 electrochemical reactor

The UA63.03 reactor studied is shown in Fig. 1A in expanded view, while Fig. 1B shows the electrochemical compartment of the cell in more detail. Table 1 shows the characteristic dimensions of this compartment. Flow distribution systems and electrode compartments were built in polypropylene and the gaskets were made of EPDM (ethylene-propylene-diene monomer (M-class) rubber).

2.1.2. The UA63.04 electrochemical reactor

The new UA63.04 reactor design was based on former UA63.03, sharing the same electrode area (63 cm^2) with an extra 1 mm thickness required for the proper mechanization of the entrance-exit manifolds. The main difference between both compartments is found in the entrance manifold, which consists of five narrow inlet nozzles as shown in Fig. 2A. The exit manifold is also modified, where two outlet nozzles have been settled at both ending corners (Fig. 2B). The main dimensions of the new compartment are also included in Table 1.

2.2. RTD experiments for the UA63.04 reactor

Experimental residence time distribution (RTD) data for the UA63.04 was obtained by the injection–response method following the same procedure described in previous works for different filter-press compartments developed at the University of Alicante [16,17,32] where a saturated KCl solution (≈3.5 M in water at room temperature) was injected upstream the entrance manifold of the reactor and conductivity was measured downstream the exit manifold. 5 mL of the KCl solution was manually injected with a 5 mL syringe where the plunger area of the syringe was comparable to the flow area of the pipe, allowing manual injections lasting 1–2 s for all the Re values studied. The syringe remained in the injection point, and the small amount of the solution retained in the plunger slowly flew through the pipe for a few seconds after the injection was made, especially for lower flow rates. Conductivity was measured by an Ingold conductivity probe connected to a Crison 522 conductimeter and a Philips PM 8133 X-t analogue recorder in order to register the variation of conductivity vs. time. Both injection and measuring points were located less than 15 cm away from the entrance and exit manifolds (polypropylene blocks with flow channels), respectively. The experimental set-up is shown elsewhere (Fig. 1b in Ref. [16]). Although KCl concentration vs. conductivity practically fits a linear regression even for high KCl concentrations near saturation [35,36], studies were restricted to the region in which the conductivity of KCl solutions was directly proportional to its concentration.

2.3. CFD simulations

2.3.1. Fluid flow and diffusion–convection equations

Fluid flow modelling is based on the conservation of mass, momentum and energy. The working liquid is water at 20 °C, and is assumed as incompressible, Newtonian and isothermal, so that its motion can be described by the two momentum and mass conservation equations [37]:

$$\rho\frac{\partial \mathbf{v}}{\partial t} - \eta\nabla^2\mathbf{v} + \rho(\mathbf{v}\cdot\nabla)\mathbf{v} + \nabla p = G \quad (1)$$

$$\nabla\cdot\mathbf{v} = 0 \quad (2)$$

where $\mathbf{v}$ is the fluid velocity field, ρ and η are the density and dynamic viscosity of the fluid, respectively, t is time, p is the fluid pressure and G are the volume forces applied on the fluid. Assuming steady state and neglecting gravity forces, the first terms of the left-hand side and right-hand side in Eq. (1) are cancelled.

Besides, in order to obtain RTD theoretical curves to be compared with experimental data, a convection–diffusion equation was solved:

$$\frac{\partial c}{\partial t} + u\frac{\partial c}{\partial x} + v\frac{\partial c}{\partial y} + w\frac{\partial c}{\partial z} = R + D\left(\frac{\partial^2 c}{\partial x^2} + \frac{\partial^2 c}{\partial y^2} + \frac{\partial^2 c}{\partial z^2}\right) \quad (3)$$

where c denotes the concentration of the species, D denotes its diffusion coefficient, u, v and w are the velocity components in the x, y and z direction and R is the chemical reaction source-term. The R term was neglected since no chemical reactions were taking place, reducing the transport of the tracer to a pure convection–diffusion case. Still, this term is an interesting feature from a chemical reaction engineering point of view as kinetics terms could be applied, becoming a useful tool to describe the performance of any chemical reactor.

2.3.2. Resolution procedure

Due to the fact that the analysis of the fluid flow inside an electrochemical filter-press reactor by CFD simulations is an

Table 2
Volumetric flow rate (Q), mean linear velocity (v), mean linear velocity at the inlet (v_{inlet}) and Re at the inlet for former UA63.03 and new UA63.04 reactors working at the Re values included in this study.

Re	UA63.03 reactor				UA63.04 reactor			
	Q (L h^{-1})	V (m s^{-1})	V_{inlet} (m s^{-1})	Re_{inlet}	Q (L h^{-1})	V (m s^{-1})	V_{inlet} (m s^{-1})	Re_{inlet}
129	17.0	2.24×10^{-2}	0.122	856	17.2	1.70×10^{-2}	0.398	1193
200	26.3	3.48×10^{-2}	0.190	1328	26.6	2.64×10^{-2}	0.617	1850
271	35.6	4.71×10^{-2}	0.257	1799	36.1	3.58×10^{-2}	0.836	2507
414	54.4	7.20×10^{-2}	0.393	2749	55.1	5.47×10^{-2}	1.277	3830

innovative technique, no standard procedure has been developed in order to characterize this kind of electrochemical systems by CFD simulations. Therefore, different approaches have been proposed in literature: (i) Jomard et al. [24] analyzed a 0.04 m × 0.013 m × 0.16 m laboratory prototype electrolyser by coupling Fluent and Flux Expert codes. They used the k–ε, Euler–Euler model for giving realistic turbulent drainage for higher Re values than 1300, but simplified geometries for the fluid inlet and outlets where uniform velocity profiles were assumed. These boundary conditions provided velocity vector plots converging towards parabolic profiles (hydraulic velocity shape characteristic of the wall effect), but no effect of the entrance–exit ports could be examined. (ii) Santos et al. [25] analyzed flow regime and mass transport in the DiaCell 106 electrolyser (projected area 63 cm^2) using the OpenFOAM CFD software package, following a monophasic methodology. Navier-Stokes equations were solved using no turbulence models for flow conditions with low Reynolds values ranging from 25 to 165, while for Re from 1200 to 2500, a turbulent approach was considered (Re was defined by using the inter-electrode distance as characteristic length). (iii) Vázquez et al. [26] analyzed a different commercial filter-press reactor (FM01-LC electrolyser with projected area 64 cm^2) using the Fluent CFD code. They chose a specific k–ε turbulence model (renormalization-group model, RNG) to solve the fluid flow equations, alleging that the model considered was appropriate for regions dominated by strong velocity gradients like recirculation flow regions, even though their studied Reynolds range was between Re = 197 and Re = 1574. The RNG k–ε turbulence model provides better results than regular k–ε turbulence models for laminar flow conditions [38], but a different approach would be desirable with laminar Reynolds values.

In this work, COMSOL Multiphysics 3.3 was used in order to simulate both hydrodynamic behaviour and tracer experiments. Laminar flow conditions were assumed in CFD simulations presented in this work considering previous works by the authors [7,17,32], where a critical Re value of 1000 was experimentally determined in order to distinguish laminar/turbulent hydrodynamic behaviour of former UA63.03 reactor. The same laminar hypothesis was assumed in an equivalent Re range by Santos et al. [25]. Still, this hypothesis can be considered controversial, and its validation is a task of the present paper. The results presented hereinafter confirm the pertinence of the assumption of laminar flow for both reactors.

A high convergence was reached for the same low Reynolds numbers (129, 200, 271 and 414, see Table 2) used in previous experimental works, where the characteristic length was the equivalent hydraulic diameter (d_e). Different mesh sizes were used in order to obtain a grid independent solution, and no significant modification of the fluid velocity was observed with deeper refinement of the employed mesh, which consisted of 25 000 tetrahedral elements in both reactors, where the damped Newton method with the GMRES (generalized minimal residual method) solver [39] was employed to solve the model equations. For tracer simulations, a solution was obtained by decoupling the transient solution of the convection–diffusion equation from the Navier-Stokes solution since steady state was assumed in the fluid flow Eqs. (1) and (2), and the presence of the tracer was assumed of negligible influence on the fluid properties.

Fig. 3 shows the UA63.03 and UA63.04 geometries, pointing out inlet and outlet boundaries, electrode and membrane (or counter-electrode when working in undivided configuration). Part of the exit manifold of the UA63.03 geometry was not taken into account in order to simplify the calculations, assuming atmospheric pressure for the outlet nozzles, as the cylindrical outlet flow distributor was not completely filled with electrolyte during real experiments. Table 3 shows the boundary conditions used for the CFD simulations. In filter-press reactors working in divided configuration, flux through the membrane may occur, but it is several orders of magnitude smaller than the channel cross-flow velocity. Therefore, the membrane was modelled as a non-permeable wall, assuming that velocity at the membrane surface is zero (no slip condition). For the tracer experiment simulation, we assumed a basic Gaussian pulse for the injection of the KCl solution considering the experimental procedure. The injection was set at the inlet boundaries of both reactors, which were considered to behave closely to perfect plug flow regime. The assumption of uniform velocity and concentration profiles simplify the boundary treatment (especially for engineering calculations), and as the fluid flow rapidly develops in the manifold for both reactors, it does not actually affect the hydrodynamic behaviour seen in the compartments.

2.3.3. Validation of CFD simulations

CFD simulations of the hydrodynamic behaviour of an electrochemical filter-press reactor have been previously validated by different methods. Santos et al. [25] validated the CFD calculations of the velocity field inside DiaCell 106 electrolyser experimental with pressure drop measurements, mass balance analyses and mass transport studies, while Vázquez et al. [27] used the fluid velocity obtained by CFD simulations on previous mass transport correlations to estimate local and global mass transport coefficients. In both cases, experimental mass transport studies were based on limiting current techniques which usually provide global mass transport coefficients. The estimation of global mass transport coefficients by local ones obtained from CFD simulations and its comparison to experimental values might seem controversial, especially when local mass transport coefficients were already obtained from local velocity profiles by empirical equa-

Table 3
Boundary conditions for CFD simulations.

Domain equations	Inlet	Outlet nozzles	Walls
Navier-Stokes	V_{inlet}	Pressure, no viscous stress: $p = 0$, $\eta(\nabla \mathbf{v} + (\nabla \mathbf{v})^T)n = 0$	No slip condition: $\mathbf{v} = (u, v, w)$
Convection–diffusion	$c = c_i e^{-t^2/A^2}$	$(D \nabla c)n = 0$	Insulation condition: $N \times n = 0$, $N = (-D \nabla c + c\mathbf{v})$

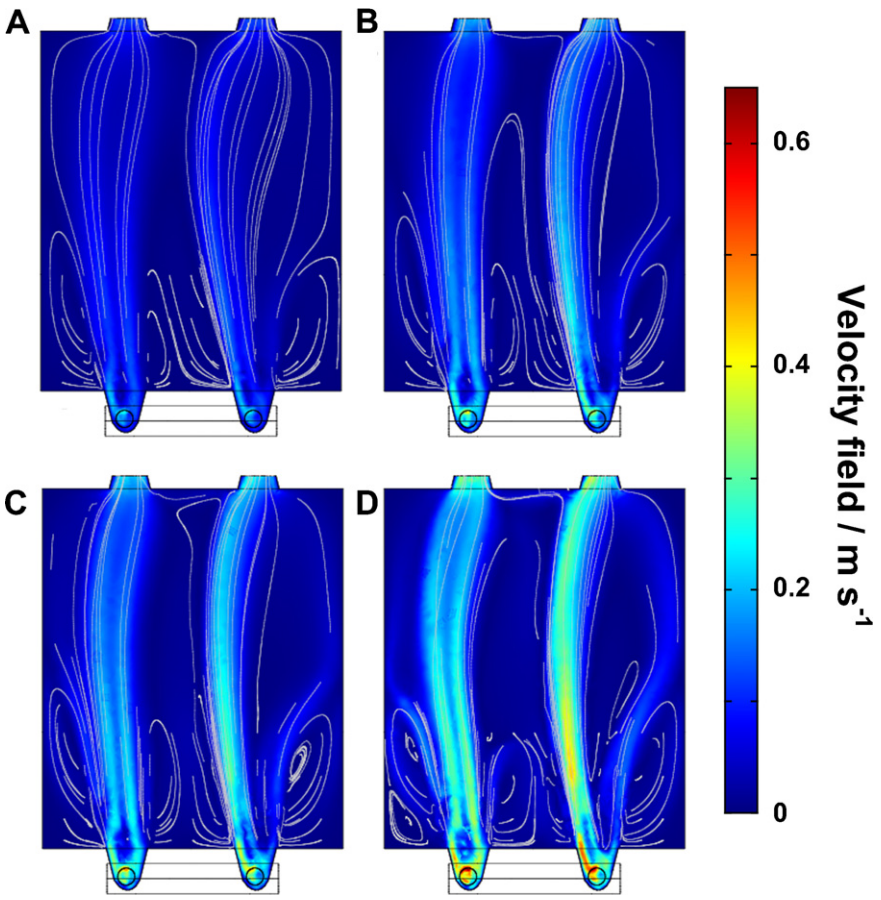

Fig. 4. CFD simulations of the UA63.03 reactor for different Re values at $z = 1.5$ mm: (A) Re = 129, (B) Re = 200, (C) Re = 271, (D) Re = 414. The velocity field ($|\mathbf{v}|$) is represented in color map ($m\,s^{-1}$). Flow direction is represented by grey streamlines. The membrane boundary lays on the $z = 0$ plane in all cases.

tions meant to predict overall reactor performances. This latter consideration was adopted by Vázquez et al. [27], who calculated local mass transport coefficients (k_m) from CFD simulations and then compared them with experimental k_m evaluated elsewhere [40], observing an increase in the deviation of numerical k_m values for increasing Re values. In contrast, Santos et al. [25] employed a more rigorous approach as they determined local k_m values on the anode by assuming that the solute mass

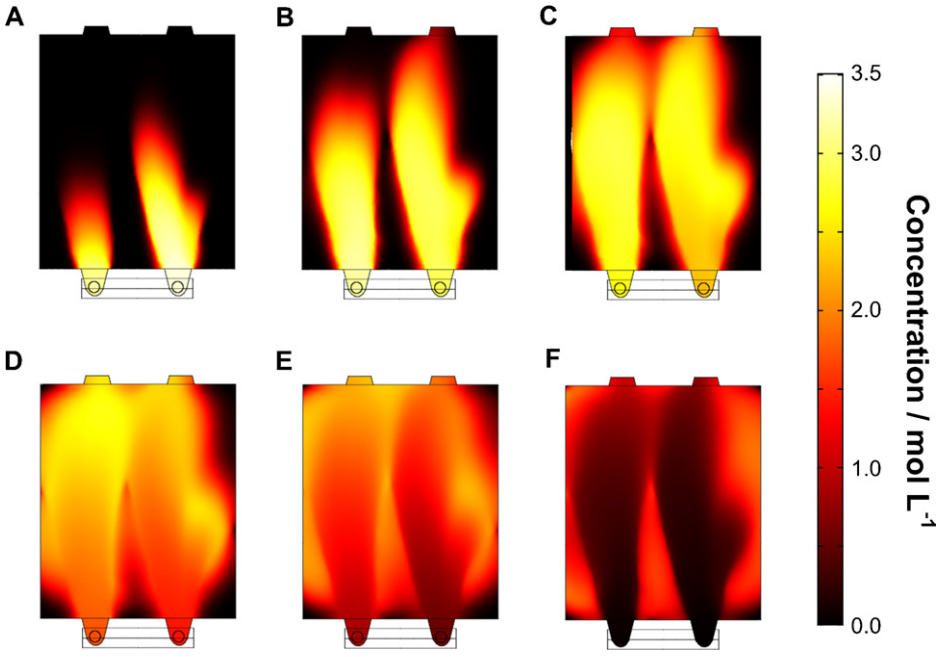

Fig. 5. Tracer diffusion simulation inside the UA63.03 reactor for Re = 129 at $z = 1.5$ mm: (A) $t = 1$ s, (B) $t = 2$ s, (C) $t = 3$ s, (D) $t = 4.5$ s, (E) $t = 6$ s and (F) $t = 9$ s. Pulse at the inlet of the reactor is a 3.5 M KCl solution. Concentration of KCl is represented in color map ($mol\,L^{-1}$). The membrane boundary lays on the $z = 0$ plane in all cases.

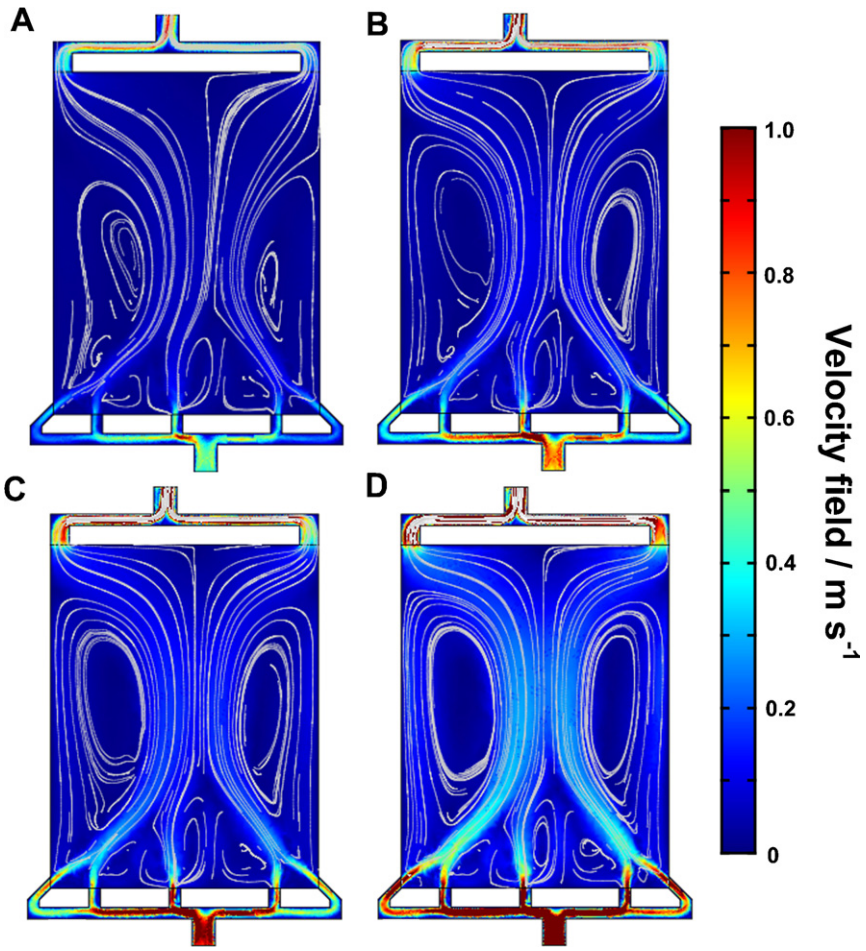

Fig. 6. CFD simulations of the UA63.04 reactor for different Re values at $z = 1.5$ mm: (A) Re = 129, (B) Re = 200, (C) Re = 271, (D) Re = 414. The velocity field ($|\mathbf{v}|$) is represented in color map ($m\,s^{-1}$). Flow direction is represented by grey streamlines. The membrane boundary lays on the $z = 0$ plane in all cases.

fraction on the electrode surface was zero. They compared calculated area-averaged k_m with those obtained with limiting current experiments, reaching a very good agreement except for a slight deviation in the lower Re range. These differences between both studies suggests that alternative methods should be considered in order to validate CFD simulations while the validity of the comparison of local/global mass transport coefficients obtained from CFD simulations to experimental global values remains unclear.

To our knowledge, there is not any comparison between experimental RTD data and calculated RTD curves obtained from CFD simulations for electrochemical filter-press reactors, despite the interesting information that can be obtained from this analysis [23]. According to this, tracer diffusion simulations were employed to obtain simulated RTD curves. Variation of the concentration vs. time at the outlet nozzles for the tracer was calculated by integration of the KCl concentration on the surface of both outlet nozzles of the UA63.03 geometry for each time step. Values were normalized with the total amount of tracer to be compared with experimental RTD data [32] in order to validate CFD simulations of former UA63.03 reactor. In addition, simulated RTD curves were also obtained for the new UA63.04 reactor to validate the CFD calculations for this reactor with RTD experiments included in this work.

3. Results and discussion

3.1. Fluid velocity and tracer diffusion

3.1.1. UA63.03 reactor

For the UA63.03 electrochemical reactor, both hydrodynamic behaviour and tracer response were obtained by COMSOL simulations for different Reynolds numbers (129, 200, 271 and 414). Fig. 4 shows the velocity field and streamlines for the different Reynolds values. For Re = 129, two main streams cross the UA63.03 compartment, each one coming from a different inlet nozzle. Three main stagnant areas are observed along the compartment, with a noticeable recirculation flow region near the entrance zone of each stagnant area, while in the second half of the reactor the flow is fully developed from the flow direction point of view. At higher Re values (200 and 271), a backward path forms between the two main streams, even though its fluid velocity remains relatively low. Also, a secondary jet builds up from the right inlet nozzle, becoming more noticeable as the flow rate is increased. This secondary jet becomes stronger for Re = 414 and, along with the main stream, encloses a different recirculation flow region. At the highest Re value, the existence of several well-defined vortices with low fluid velocity located in the first half of the compartment is clearly seen, where mass transfer is expected to occur between the main streams and stagnant zones. This feature is confirmed by Fig. 5, which shows

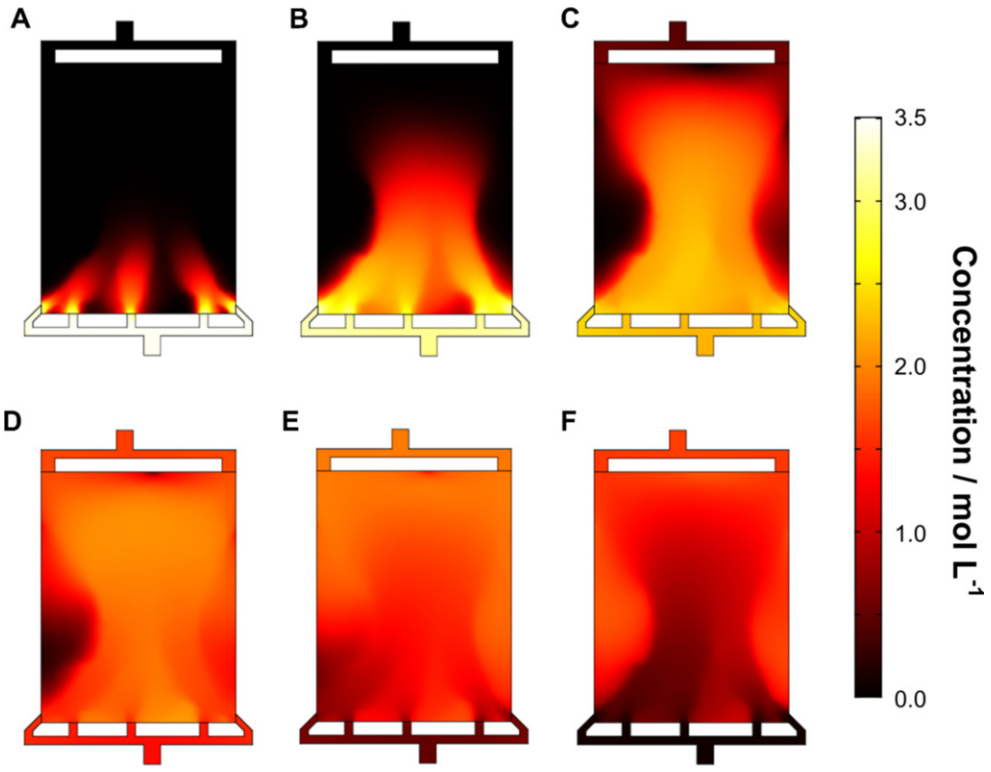

Fig. 7. Tracer diffusion simulation inside the UA63.04 reactor for Re = 129 at z = 1.5 mm: (A) t = 0.5 s, (B) t = 1.5 s, (C) t = 3 s, (D) t = 4.5 s, (E) t = 6 s and (F) t = 8 s. Pulse at the inlet of the reactor is a 3.5 M KCl solution. Concentration of KCl is represented in color map (mol L^{-1}). The membrane boundary lays on the z = 0 plane in all cases.

the tracer evolution vs. time for Re = 129 (animated films for tracer simulations inside the reactor working at each Re value studied are included as Supplementary data). The tracer goes preferentially through the reactor following the main paths predicted by hydrodynamic simulations, and mass exchange occurs between the main paths and the stagnant zones caused by recirculation flow. This is frequently observed in several hydrodynamic systems with stagnant or dead volumes such as shallow cavities in channels [41], where most of the mass exchange between cavity and channel takes place where large spanwise vortices are shed in laminar conditions.

3.1.2. UA63.04 reactor

The hydrodynamic behaviour and tracer response inside the new UA63.04 reactor was also obtained for the same Reynolds numbers (129, 200, 271 and 414). Fig. 6 displays the fluid velocity and flow direction for this reactor. As expected, one jet comes from each inlet nozzle and the fluid velocity quickly decreases as fluid flow develops with the five jets forming a main stream crossing the UA63.04 compartment for all the Re values studied. When the main stream flows towards the outlet side, it divides into two paths, and each one also splits up into two jets: one leaves the reactor via the nozzles located at each corners of the outlet side while the other comes back along the outer edges of the compartment, becoming more notorious as the flow rate is increased. Apparently, five stagnant areas are observed: the main two zones are located between the backward jets and the main stream, another two are placed between the three interior inlet nozzles and the last one remains in the middle of the outlet side. The interest of these stagnant areas (excluding the one located in the middle of the outlet side) lies in the presence of recirculation flow where mass exchange is expected (the presence of well-defined vortices is observed in Fig. 6). This feature is confirmed by tracer-diffusion simulations as shown in Fig. 7 (animated films for tracer simulations inside the UA63.04 reactor working at each studied Re may also be found as Supplementary data). It shows how the tracer follows the main paths predicted by CFD hydrodynamic simulation and how mass exchange occurs between the main paths and the vortices located at the stagnant zones.

3.2. Validation with simulated RTD curves

3.2.1. UA63.03 reactor

Fig. 8 shows the experimental and simulated RTD data for the UA63.03 reactor working at different Re values. All of them show that the tracer front exits the reactor earlier than the average residence time ($t_{average}$). In addition, long tails are observed for all the Re values. Both features indicate that former UA63.03 reactor behaves as a combination of a plug flow with axial dispersion and flow exchange with stagnant zones as stated in previous works [32], reaching a good agreement between experimental and simulated RTD data. The following error estimation was used:

$$\text{error} = \frac{\sum (y_{exp} - y_{calc})^2}{N} \quad (4)$$

where y_{exp} and y_{calc} are the experimental and calculated RTD data and N is the total number of data points, giving an estimated error lower than 4×10^{-4}. This good agreement between experimental and simulated data supports the validity of CFD simulations and in particular, the election of a laminar model to estimate the hydrodynamic behaviour inside the UA63.03 electrochemical reactor in the studied Re range.

In addition, the study of simulated local RTD curves enables to study the behaviour of those stagnant areas that have been previously defined with the help of velocity field plots where poor electrolyte renewal is expected. According to Fig. 9, four different zones inside the electrochemical reactor compartment were analyzed: the left inlet side corner and the right inlet side cor-

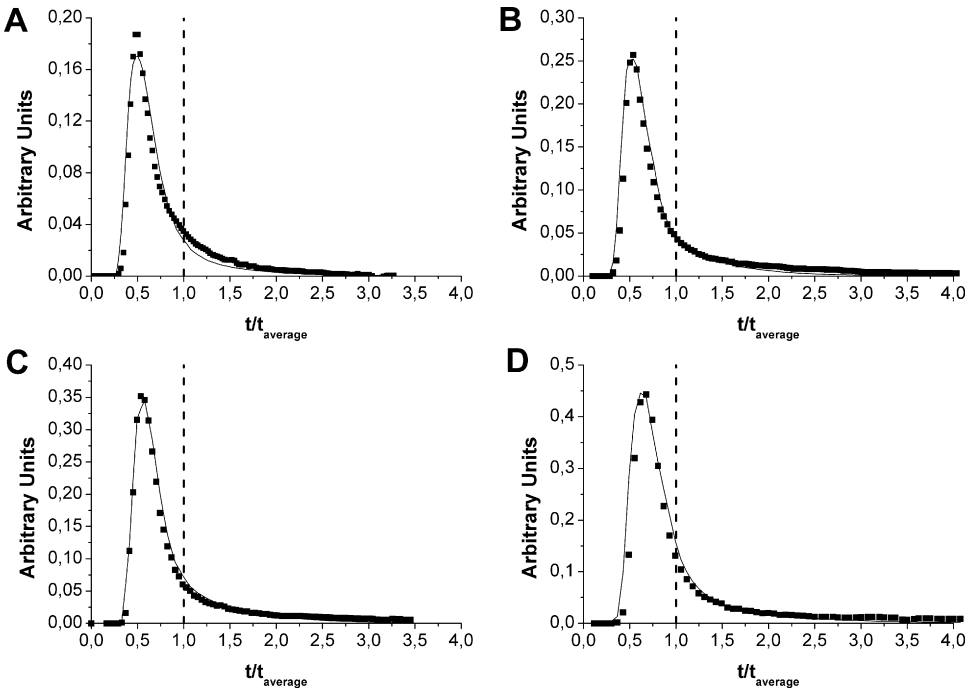

Fig. 8. Experimental (■) and simulated (—) normalized RTD values for the UA63.03 reactor for different Reynolds numbers: (A) Re = 129, (B) Re = 200, (C) Re = 271, (D) Re = 414. The vertical dashed line designates $t_{average}$.

ner (which were expected to show a stagnant behaviour based on Fig. 4), and two points right next to both inlet nozzles, as it is indicated in the graph insets. The tracer response near the inlet nozzles shows a very small retention of tracer with time as expected. However, concentration vs. time curves show a very large tail in the zones located near the corners of the compartment, which means that the tracer takes longer to leave these areas, clearly indicating a slow mass exchange between the latter and the main flow.

3.2.2. UA63.04 reactor

Comparison of experimental and simulated RTD data was also carried out to check the validation of the CFD simulations for the new UA63.04 reactor. Fig. 10 displays experimental and simulated normalized RTD curves. In contrast to what was observed for former UA63.03 reactor, the tracer front takes longer than $t_{average}$ to exit the UA63.04 reactor for all the Re studied, which means that the design of the exit–entrance manifolds yields strong recirculation flow inside the reactor, making the tracer to stay significantly

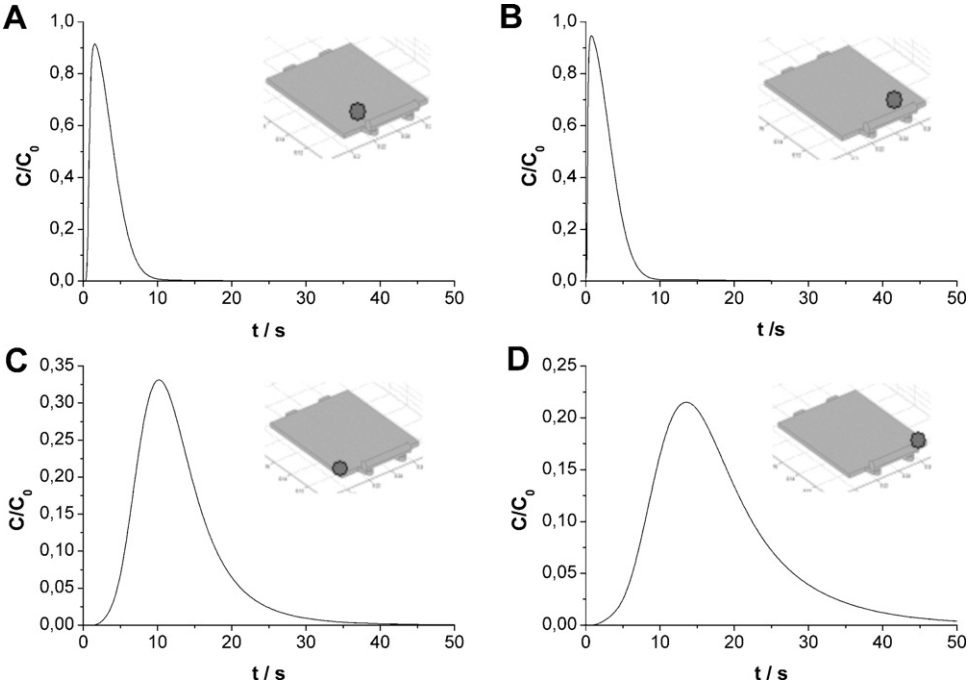

Fig. 9. CFD study of tracer concentration variation with time at four different locations inside the UA63.03 compartment working at Re = 129: (A) area near the left inlet nozzle, (B) area near the right inlet nozzle, (C) area near the left inlet side corner, (D) area near the right inlet side corner.

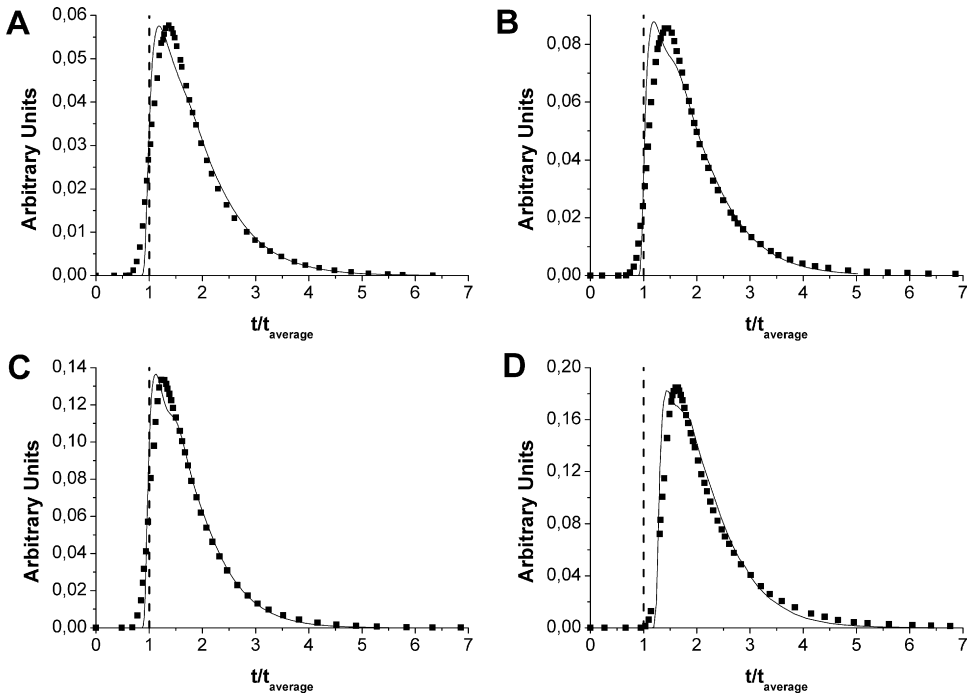

Fig. 10. Experimental (■) and simulated (—) normalized RTD values for the UA63.04 reactor for different Reynolds numbers: (A) Re = 129, (B) Re = 200, (C) Re = 271, (D) Re = 414. The vertical dashed line designates $t_{average}$.

longer in the UA63.04 reactor than in the UA63.03 reactor from the $t_{average}$ point of view. However, this behaviour does not mean that the UA63.04 reactor works under undesired conditions, because (i) the velocity field is more homogeneous in the UA63.04 reactor than in former UA63.03 cell as the RTD curves are quite more symmetric for the new reactor, and (ii) tails observed in Fig. 8 point that the stagnant volume stays over 5–6 times longer than the front in former UA63.03 reactor, while stagnant volume in the UA63.04 cell stays 3–4 times longer than the front (Fig. 10), implying that tracer retention in stagnant areas is greater in former UA63.03 reactor. Again, a good agreement was obtained for the different Re numbers. The estimated error was lower than 2.8×10^{-4}, supporting the validity of the CFD simulations and the election of a laminar model.

Simulated local RTD curves were again studied, providing an accurate description of the active and stagnant zones previously observed in Fig. 6. Fig. 11 shows the variation of the tracer concentration vs. time at seven different areas within the reactor compartment. Contrary to what was observed for former UA63.03 reactor (Fig. 9), the length of the tails is quite similar in all areas, including those zones located near the vortices where stagnant behaviour is expected (Fig. 11F and G). In addition, two noticeable peaks appear near both inlet side corners (Fig. 11D and E). The appearance of those peaks is due to the effect of the presence of the inlet jet which ends up forming the main stream with the others (first peak observed) and the jets that come back to the inlet side along the outer edges of the compartment (second peak observed). Compared to the UA63.03 reactor, the curves obtained for the analyzed stagnant areas show a relatively smaller retention of tracer with time, as tails are relatively shorter. Therefore, areas where stagnant behaviour was expected have been significantly reduced in the UA63.04 compartment compared with those observed in the UA63.03 reactor.

3.3. Ratio of active areas inside the reactors

As commented in previous sections, fast and slow zones were clearly observed inside the both reactors. Therefore, the consideration of an electrode working homogeneously is far from being accurate, evidencing the need to locate and quantify the regions where electrodes are poorly working.

In previous works by the authors [32], the ratio of active zones inside the reactor was calculated as "the ratio between volume in dispersed plug flow and total volume" of the reactor (parameter Φ_β), which was numerically obtained for the UA63.03 reactor using experimental RTD curves and employing a mathematical model [16–18,32]. However, with CFD simulations we can actually define the ratio of stagnant areas as the relation between those regions where the velocity field stays above a certain value and the total volume of the reactor. By defining stagnant zones inside the UA63.03 reactors as those where the velocity field stays below the 45% of the mean linear velocity corresponding to each Re value, we obtained the minimum error between parameter Φ_β and the newly defined ratio of stagnant areas inside the UA63.03 reactor (Table 4). Although this value may sound arbitrary, its consideration is actually in concordance with the classical definition of the cut-off point in RTD curves [42] used to assess whether the fluid flowing through any chemical reactor is active or stagnant, as stagnant volume is considered to stay over twice the average residence time, meaning that stagnant flow is twice slower than the fluid which actually moves at the mean linear velocity inside the reactor. For the UA63.03 reactor, about 40% of the total volume of the reactor was working under undesired behaviour at lower Re, and only at the highest Re number (414) the active zones inside the system increased up to 74% of the total volume. Still, 26% of the electrode area was not working under proper conditions from the fluid velocity point of view, meaning that undesirable processes such as

Table 4
Ratio of active areas inside the UA63.03 reactor calculated by RTD and CFD studies.

Re	Φ_β (%)	Active areas (%)	Error (%)
129	58	63	7.9
200	58	55	5.5
271	59	55	7.3
414	74	74	0.0

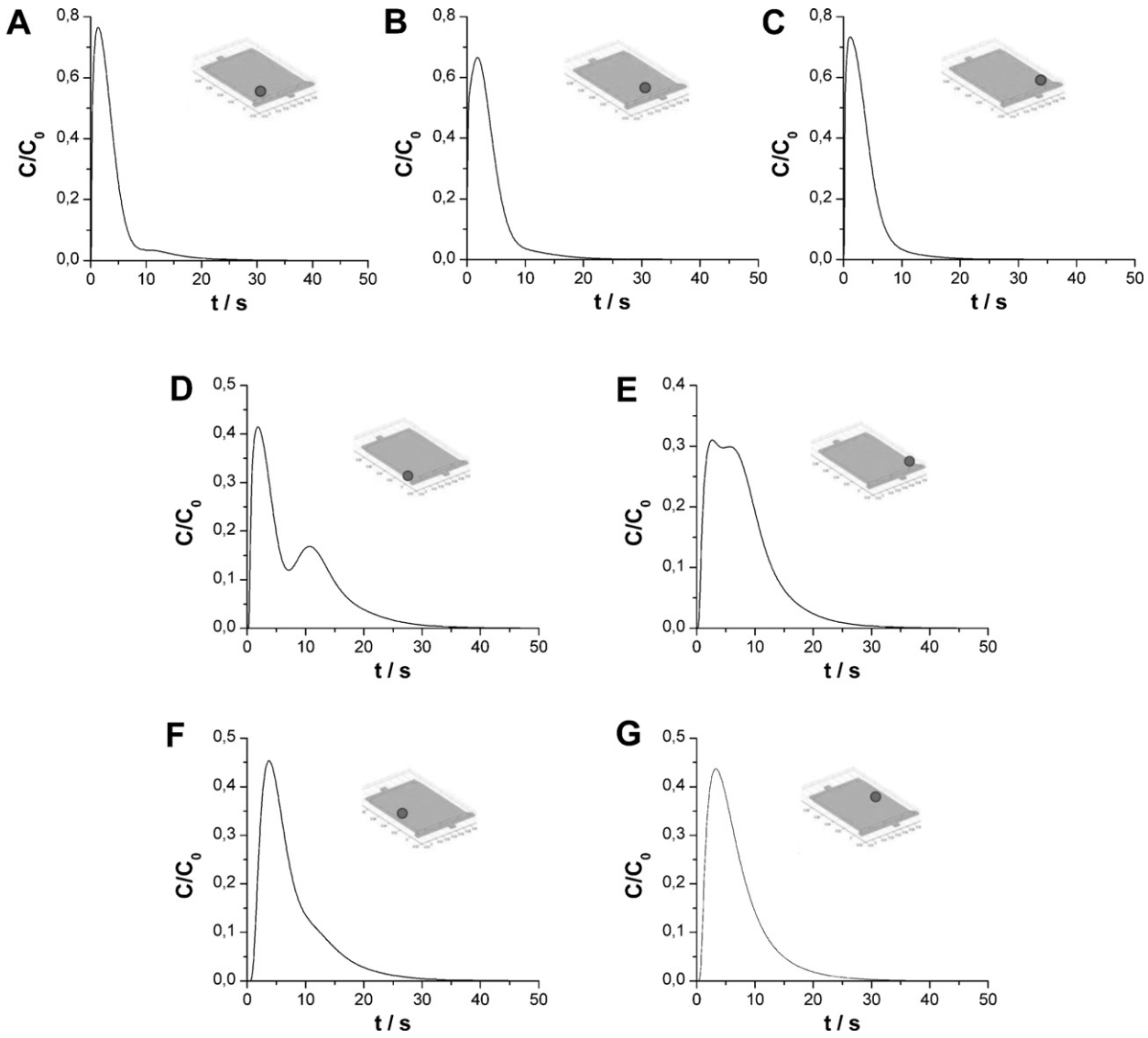

Fig. 11. CFD study of tracer concentration variation with time at four different locations inside the UA63.04 compartment working at Re = 129: (A) area near the inner left inlet nozzle, (B) area near the centered inlet nozzle, (C) area near the inner left inlet nozzle, (D) area near the left inlet side corner, (E) area near the right inlet side corner, (F) area near left vortex, (G) area near right vortex.

gas-evolving reactions or electrode corrosion could take place on a short and long-term basis. Other commercial filter-press reactors such as the DiaCell 106 electrolyser present the same non-optimal behaviour observed for the UA63.03 at an equivalent Re range [25] while other reactors such as the FM01-LC reach a slightly more uniform distribution of active areas [26], where part of the reactor would act as a calming zone where the fluid flow develops.

However, the new UA63.04 compartment presented a completely different behaviour compared with the previously mentioned reactors. The ratio of active areas inside the compartment related to the total volume of the reactor was also calculated for the UA63.04 cell following the same procedure used for the UA63.03 reactor, where active areas were again defined as those where local velocity stayed above 45% of the theoretical velocity corresponding to each Reynolds number. Table 5 compares the ratio of active areas inside both UA63.04 and former UA63.03 reactors, showing that most of the UA64.04 reactor works under desired behaviour, reaching an outstanding performance in all the Reynolds values studied, as active areas are over 90% of the reactor with no significant dependence on the Reynolds values. This statement can be clearly seen in Fig. 12, where isocurves plots for both reactors working at Re = 129 are shown. The lower velocity isocurve represents the areas where the velocity field is above 45% of the mean linear velocity inside de compartment. It is clearly seen that empty zones which represent stagnant areas are much more predominant in former UA63.03 reactor than in the newly designed UA63.04 cell, where the stagnant zones are mainly located at the main vortices previously reported.

Table 5
Calculated ratio of active areas for the new UA63.04 and former UA63.03 electrochemical reactors.

Re	Ratio of active areas (%)		Increase in ratio of active areas (%)
	UA63.03	UA63.04	
129	63	91	44
200	55	92	67
271	55	92	67
414	74	93	25

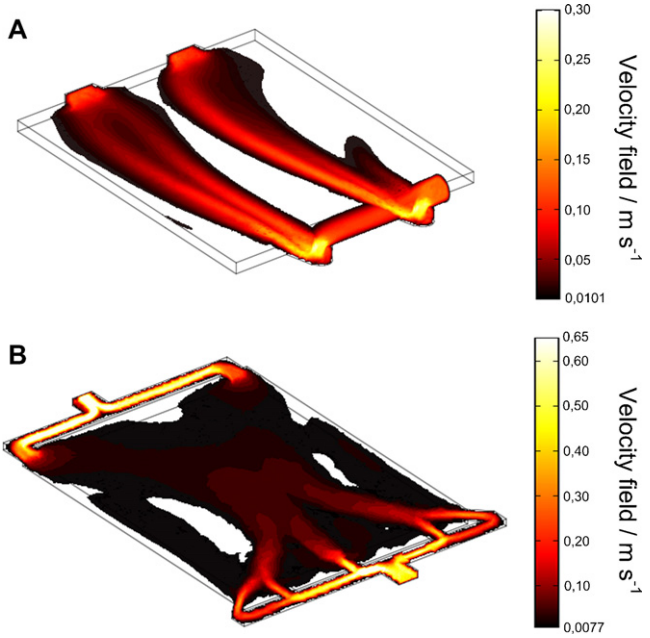

Fig. 12. Velocity field isocurves for (A) former UA63.03 and (B) newly designed UA63.04 reactors working at Re = 129. Empty zones designate stagnant zones within compartments, while isocurves designate active zones where $|\mathbf{v}| > 0.45V$.

4. Conclusions

CFD simulations can provide a detailed knowledge of the velocity flow distribution inside the electrochemical reactor compartments. A proper treatment of the fluid velocity data obtained from CFD simulations by electrochemical engineers provides interesting information related to the performance of electrochemical filter-press reactors, reducing the need for preliminary experimental tests in order to check the feasibility of new compartment designs. In this work, tracer diffusion has also been taken into account by coupling the Navier-Stokes solution to the convection–diffusion equation, in order to simulate RTD curves.

Regarding the electrochemical filter-press reactors studied in this work, the hydrodynamic characterization and modellization of former UA63.03 and new UA63.04 reactors by CFD simulations was validated using experimental RTD from previous work:

1. Simulated RTD curves, based on CFD simulations, were obtained and compared with experimental RTD data for the studied compartments, and a good agreement was found. Moreover, CFD simulations went even further than regular RTD studies, as they did not just point out the existence of dead volumes or stagnant zones inside the reactor, but also located those stagnant areas where undesirable processes could take place.
2. The fluid velocity field obtained by CFD simulations enabled to observe the reactor areas working correctly and the inactive zones where undesirable secondary reactions can occur due to the local depletion of electroactive species. The ratio of active zones was calculated from the same CFD simulations and compared with previous results calculated by RTD modellization for the UA63.03 reactor. The good agreement between both results appears as a good validation of CFD simulations. For UA63.03 reactor, the results also showed that at least 26% of the electrode area was not working under desired conditions. However, the new UA63.04 showed an optimal behaviour, as more than 90% of the reactor was working in proper conditions, improving the reactor performance and avoiding harmful processes that could lead to the corrosion of the electrode and the formation of undesired by-products.
3. The experimental validation of the CFD simulations with RTD curves confirms the pertinence of solving the Navier-Stokes equations under the hypothesis of laminar flow instead of using a turbulence model in the studied Re range.

The optimization of former UA63.03 electrochemical reactor has been accomplished with the new UA63.04 reactor, where the entrance–exit manifolds were completely re-designed while keeping the same electrode area (63 cm^3). With the new reactor, two main goals were achieved: (i) a greater percentage of actives zones with low dependence on the Re value, which improves the electrode behaviour, and (ii) a more uniform distribution of the fluid velocity, which also should improve the overall electrochemical reactor performance. The latter statement must now be validated with mass transport studies for the UA63.04 reactor, and experimental work based on limiting current techniques is on its way.

Acknowledgments

A.F.-F., V.S. and J.G.-G. thank to Generalidad Valenciana for its financial support under project GV05/104. J.G.-G. thanks to the Ministry of Industry, Tourism and Trade for its financial support under contract DEX-560620-2008-135. J.G.-G. and I.T. thank to Generalidad Valenciana for its financial support under project ACOMP09/128 and grant FPA/2009/024. M.D.E. thanks Caja de Ahorros del Mediterraneo for her pre-doctoral grant. O.L. and J.G.-G. thank the Universidad de Alicante and Generalidad Valenciana for their support in scientific exchange missions.

Appendix A.

List of symbols and abbreviations

B	compartment width (m)
c	tracer concentration (mol m^{-3} or M, mol L^{-1})
CFD	computational fluid dynamics
d_e	equivalent (hydraulic) diameter of the compartment (m), $d_e = 2Bs/(B+s)$
D	diffusion coefficient (m^2 s^{-1})
FEM	finite elements method
G	external forces (N m^{-3})
L	length of the compartment in the direction of flow (m)
Le	dimensionless length group, $Le = d_e/L$
p	pressure (Pa)
R	reaction term (mol m^{-3} s^{-1})
Re	Reynolds number, $Re = v_{lin}\rho d_e/\eta$
RTD	residence time distribution
s	separation between the membrane and the electrode (m)
t	time (s)
$t_{average}$	average residence time (s)
u	velocity component in the x direction (m s^{-1})
Q	volumetric flow rate (L h^{-1})
v	velocity component in the y direction (m s^{-1})
$\mathbf{v}$	fluid velocity field (m s^{-1}), $\mathbf{v} = (u, v, w)$
V	mean linear fluid velocity in the compartment (m s^{-1})
V_{inlet}	mean linear fluid velocity in the reactor inlet (m s^{-1})
w	velocity component in the z direction (m s^{-1})

Greek letters

Φ_β	ratio between volume in dispersed plug flow and total volume
γ	aspect ratio, $\gamma = s/B$
ρ	density (kg m^{-3})
η	dynamic viscosity (Pa s)

Appendix B. Supplementary data

Supplementary data associated with this article can be found, in the online version, at doi:10.1016/j.cej.2011.02.053.

References

[1] J. Pickett, Electrochemical Reactor Design, Elsevier, Amsterdam, 1979.
[2] F. Coeuret, A. Storck, Eléments de Génie Electrochimique, Tec-Doc Lavoisier, Paris, 1984.
[3] T.V. Nguyen, C.W. Walton, R.E. White, J. Van Zee, Parallel-plate electrochemical reactor model, J. Electrochem. Soc. 133 (1986) 81–87.
[4] D. Pletcher, F.C. Walsh, Industrial Electrochemistry, Chapman and Hall, London, 1990.
[5] F.C. Walsh, G.W. Reade, Design and performance of electrochemical reactors for efficient synthesis and environmental treatment. Part 2. Typical reactors and their performance, Analyst 119 (1994) 797–803.
[6] A.A. Wragg, A.A. Leontaritis, Local mass transfer and current distribution in baffled and unbaffled parallel plate electrochemical reactors, Chem. Eng. J. 66 (1997) 1–10.
[7] A. Frías-Ferrer, J. González-García, V. Sáez, C. Ponce de León, F.C. Walsh, The effects of manifold flow on mass transport in electrochemical filter-press reactors, AlChE J. 54 (2008) 811–823.
[8] J.M. Bisang, Effect of mass transfer on the current distribution in monopolar and bipolar electrochemical reactors with a gas-evolving electrode, J. Appl. Electrochem. 23 (1993) 966–974.
[9] R.E.W. Jansson, N.R. Tomov, The dehydrodimerisation of diethyl malonate in six different designs of cell, Electrochim. Acta 25 (1980) 497–503.
[10] A.M. Couper, D. Pletcher, F.C. Walsh, Electrode materials for electrosynthesis, Chem. Rev. 90 (1990) 837–865.
[11] V. Montiel, V. García-García, J. González-García, J.R. Pérez-Mallol, G. Sanchez-Cano, A. Aldaz, Étude de viabilité d'un traitement des eaux résiduaires industrielles par voie electrochimique. Un exemple réel, J. New Mater. Electrochem. Syst. 3 (2000) 269–274.
[12] A. Montillet, J. Comiti, J. Legrand, Application of metallic foams in electrochemical reactors of filter-press type Part I: flow characterization, J. Appl. Electrochem. 23 (1993) 1045–1050.
[13] P. Trinidad, F.C. Walsh, Hydrodynamic behaviour of the FM01-LC reactor, Electrochim. Acta 41 (1996) 493–502.
[14] C. Bengoa, A. Montillet, P. Legentilhomme, J. Legrand, Flow visualization and modelling of a filter-press type electrochemical reactor, J. Appl. Electrochem. 27 (1997) 1313–1322.
[15] C. Bengoa, A. Montillet, P. Legentilhomme, J. Legrand, Characterization and modeling of the hydrodynamic behavior in the filter-press-type FM01-LC electrochemical cell by direct flow visualization and residence time distribution, Ind. Eng. Chem. Res. 39 (2000) 2199–2206.
[16] J. González-García, V. Montiel, A. Aldaz, J.A. Conesa, J.R. Pérez, G. Codina, Hydrodynamic behavior of a filter-press electrochemical reactor with carbon felt as a three-dimensional electrode, Ind. Eng. Chem. Res. 37 (1998) 4501–4511.
[17] J. González-García, A. Frías-Ferrer, E. Expósito, V. Montiel, A. Aldaz, J.A. Conesa, Characterization of an electrochemical pilot-plant filter-press reactor by hydrodynamic and mass transport studies, Ind. Eng. Chem. Res. 39 (2000) 1132–1142.
[18] J. González-García, A. Frias-Ferrer, V. Montiel, J.A. Conesa, A. Aldaz, Development of a model for the characterization of fluid dispersion in electrochemical reactors, J. Hydroinform. 4 (2002) 281–295.
[19] N.G. Carpenter, E.P.L. Roberts, Mass transport and residence time characteristics of an oscillatory flow electrochemical reactor, in: A.A. Wragg (Ed.), 5th European Symposium on Electrochemical Engineering, I. Chem.E. Symp. Ser. 149, Institution of Chemical Engineers, Rugby, 1999, pp. 309–318.
[20] A. Frías-Ferrer, J. González-García, J.A. Conesa, E. Gadea-Ramos, E. Expósito, V. García-García, V. Montiel, A. Aldaz, Characterization of an electrochemical industrial size filterpress reactor by hydrodynamic and mass transport studies, in: J.P. Leclerc (Ed.), Tracers and Tracing Methods, Récent Progrès en Génie des Procédés, vol. 15 No 79, Société Française de Génie des Procédés, Nancy, 2001, pp. 205–212.
[21] G. Nelissen, G. Weyns, P. Maciel, J. Deconinck, O. Vande Vyver, H. Deconinck, Numerical study of the influence of the anode position and the electrolyte flow on the deposition of copper on a wire, Electrochim. Acta 52 (2007) 6584–6591.
[22] E.P. Rivero, P. Granados, F.F. Rivera, M. Cruz, I. González, Mass transfer modelling and simulation at a rotating cylinder electrode (RCE) reactor under turbulent flow for copper recovery, Chem. Eng. Sci. 65 (2010) 3042–3049.
[23] S.A. Martínez-Delgadillo, H. Mollinedo-Ponce, V. Mendoza-Escamilla, C. Barrera-Díaz, Residence time distribution and back-mixing in a tubular electrochemical reactor operated with different inlet flow velocities, to remove Cr(VI) from wastewater, Chem. Eng. J. 165 (2010) 776–783.
[24] F. Jomard, J.P. Feraud, J. Morandini, Y. Du Terrail Couvat, J.P. Caire, Hydrogen filter press electrolyser modelled by coupling fluent and flux expert codes, J. Appl. Electrochem. 38 (2008) 297–308.
[25] J.L.C. Santos, V. Geraldes, S. Velizarov, J.G. Crespo, Characterization of fluid dynamics and mass-transfer in an electrochemical oxidation cell by experimental and CFD studies, Chem. Eng. J. 157 (2010) 379–392.
[26] L. Vázquez, A. Alvarez-Gallegos, F.Z. Sierra, C. Ponce de León, F.C. Walsh, Simulation of velocity profiles in a laboratory electrolyser using computational fluid dynamics, Electrochim. Acta 55 (2010) 3437–3445.
[27] L. Vázquez, A. Alvarez-Gallegos, F.Z. Sierra, C. Ponce de León, F.C. Walsh, Prediction of mass transport profiles in a laboratory filter-press electrolyser by computational fluid dynamics modelling, Electrochim. Acta 55 (2010) 3446–3453.
[28] J.A. Poquis, V. García-García, J. González-García, V. Montiel, A. Aldaz, Partial electro-neutralisation of D-α-*p*-hydroxyphenylglycine in sulphuric acid medium, J. Membr. Sci. 170 (2000) 225–233.
[29] J. Iniesta, E. Expósito, J. González-García, V. Montiel, A. Aldaz, Electrochemical treatment of industrial wastewater containing phenols, J. Electrochem. Soc. 149 (2002) D57–D62.
[30] V. Sáez, M.D. Esclapez, I. Tudela, P. Bonete, J. González-García, Electrochemical degradation of perchloroethylene in aqueous media: influence of the electrochemical operational variables in the viability of the process, Ind. Eng. Chem. Res. 49 (2010) 4123–4131.
[31] A.P. Beltrá, P. Bonete, J. González-García, V. García-García, V. Montiel, Electrochemical synthesis of L-histidinol using solvated electrons, J. Electrochem. Soc. 152 (2005) D65–D68.
[32] J. Gonzalez-Garcia, J.A. Conesa, J. Iniesta, V. Garcia-Garcia, V. Montiel, A. Aldaz, Characterization of an electrochemical laboratory filterpress reactor by hydrodynamic and mass transport studies, in: A.A. Wragg (Ed.), 5th European Symposium on Electrochemical Engineering, I. Chem. E. Symp. Ser. 149, Institution of Chemical Engineers, Rugby, 1999, pp. 51–60.
[33] A. Frías-Ferrer, J. González-García, V. Sáez, J. Iniesta, V. Montiel, A. Aldaz, Hydrodynamics of electrochemical filter press reactors: a computational fluid dynamic (CFD) approach, in: Proc. 7th European Symposium on Electrochemical Engineering, Toulouse, 3–5 Oct., 2005, pp. 567–572.
[34] M. Shakaib, S.M.F. Hasani, M. Mahmood, CFD modelling for flow and mass transfer in spacer-obstructed membrane feed channels, J. Membr. Sci. 326 (2009) 270–284.
[35] G. Prentice, Electrochemical Engineering Principles, Prentice-Hall, Englewood Cliffs, 1991, p. 16.
[36] I.N. Levine, Physical Chemistry, 5th ed., McGraw-Hill, New York, 2003, p. 510.
[37] R.B. Bird, W.E. Stewart, E.R. Lightfoot, Transport Phenomena, Wiley, New York (1960).
[38] D. Choudhury, Introduction to the Renormalization Group Method and Turbulence Modeling, Technical Memorandum TM-107, Fluent Inc., Lebanon, 1993.
[39] Y. Saad, M.H. Schultz, GMRES: a generalized minimal residual algorithm for solving nonsymmetric linear systems, SIAM J. Sci. Stat. Comp. 7 (1986) 856–869.
[40] C.J. Brown, D. Pletcher, F.C. Walsh, J.K. Hammond, D. Robinson, Local mass transport effects in the FM01 laboratory electrolyser, J. Appl. Electrochem. 22 (1992) 613–619.
[41] K. Chang, G. Constantinescu, S. Park, Analysis of the flow and mass transfer processes for the incompressible flow past an open cavity with a laminar and a fully turbulent incoming boundary layer, J. Fluid Mech. 561 (2006) 113–145.
[42] O. Levenspiel, K.B. Bischoff, Patterns of flow in chemical process vessels, in: T.B. Drew, J.W. Hoopes, T. Vermeulen (Eds.), Advances in Chemical Engineering, vol. 4, Academic Press, New York, 1963, pp. 95–198.